16th World Conference on Earthquake, 16WCEE 2017
Santiago Chile, January 9th to 13th 2017
Paper N° 994
Registration Code: S-C1463410770

ANALYSIS OF FRP RETROFITTED TIMBER PILES UNDER MULTI-HAZARD LOADING

K. E. Kim[(1)], B. Andrawes[(2)]

[(1)] *Graduate Research Assistant, Department of Civil and Environmental Engineering, University of Illinois at Urbana-Champaign, Urbana, IL, 61801, kekim2@illinois.edu*
[(2)] *Associate Professor, Department of Civil and Environmental Engineering, University of Illinois at Urbana-Champaign, Urbana, IL, 61801, andrawes@illinois.edu*

Abstract

Damage to many structures in the 2004 Indian Ocean Earthquake, and the 2011 Tohoku Earthquake was caused by the seismic loading followed by tsunami inundation. Whereas countless research studies have focused on the performance of reinforced concrete and steel structures, heavy timber structures have received very little attention. This study focuses on the multi-hazard performance of timber pile bridge substructure. Most timber pile bridges currently in service in the United States were constructed in the 1950's and 60's based on now outdated design methods. Given their age and susceptibility to deterioration, the performance of timber pile bridges under extreme loading scenarios is a concern. Wrapping timber piles with fiber reinforced polymer (FRP) composites has been shown to significantly improve the strength and durability of deteriorated timber piles. In this study, a step-wise analysis method is used to subject a typical timber pile bridge substructure to a combination of earthquake and tsunami loading. The performance of unretrofitted and FRP retrofitted timber piles are compared. Being able to simulate and predict the response and failure mechanisms in these extreme natural hazards will allow for safer new designs and effective retrofits for existing structures.

Keywords: Timber Pile, Bridges, Tsunami, Seismic, FRP Retrofit

1. Introduction

Timber piles are used to support many different types of structures across North America. One of the most common uses of round timber piles is in bridges. Typical timber pile bridges consist of substructure supported by timber piles with reinforced concrete (RC) superstructure. They are generally limited to one to three spans and are used mainly on low-volume roads. Many of the existing timber pile bridges were constructed in the 1950's and 60's based on now outdated design methods which only considered concentric gravity loads. As a result, many timber pile bridges may lack the structural capacity and redundancy to resist unexpected loading scenarios.

Recent natural hazard events such as the 2004 Indian Ocean Earthquake, and the 2011 Tohoku Earthquake both of which were followed by massive tsunamis, demonstrated the destruction that can ensue from multiple hazards. While many studies have focused on the seismic performance of various structures over the years, few studies exist in the literature on multi-hazard loading. Furthermore, compared to steel and RC structures, research on the behavior and performance of heavy timber structures such as timber pile bridges is generally lacking.

In addition to inadequate design, deterioration poses a significant problem for timber pile bridges. In many cases, because timber pile bridges in lower traffic areas are not perceived as critical infrastructure, they are afforded minimal maintenance efforts. Timber decay and degradation can lead to significant reductions in strength [1, 2]. In recent years, fiber reinforced polymer (FRP) composites have become a popular option in structural rehabilitation due to their high strength-to-weight ratio, durability, and versatility. Studies have shown that FRP retrofitting can significantly improve the stiffness and strength of timber structures [3, 4].

This study uses the Open System for Earthquake Engineering Simulation (OpenSees) analysis framework to study the performance of a typical timber pile bridge bent under an earthquake-tsunami event. OpenSees is a widely used open source software framework for analyzing the seismic response of structural systems [5]. Recently, OpenSees was extended to solve fluid-structure interaction (FSI) problems using the particle finite element method (PFEM) [6]. This new capability is used to simulate an idealized tsunami. The multi-hazard analysis framework developed by Carey et al. (2014) was used to analyze the performance of a timber pile bridge bent under a sequential earthquake-tsunami event [7]. The damage caused by the loads imposed by each hazard was quantified by the resulting level of inelastic deformation and the performance of unretrofitted and FRP wrapped timber piles is compared.

2. Timber Pile Bridge Model

Timber pile bridges in the US are predominantly found in low-traffic areas and typically consist of one to three simply supported spans. The most common timber bridge configuration consists of timber pile abutments and bents with RC pile caps and precast concrete superstructure. Most timber bridge designs are closely based on the Federal Highway Administration (FHWA) Standard Plans [8]. In general, the design of the timber piles simply consisted of specifying the minimum required axial capacity with typical construction drawings specifying that test piles be driven in the field to determine the adequacy. No other design considerations were made. As a result of this simplified design approach, timber pile bridges may not have the robustness to withstand extreme loading scenarios.

In this study only an intermediate timber pile bent is considered. Based on a survey of construction drawings of existing timber pile bridges in the state of Illinois, the model timber pile bent was assumed to be 10.668 m wide with seven round timber piles. A precast concrete slab-beam superstructure 0.406 m thick was used. The pile is driven to a depth of 4.572 m and extends 2.134 m from the ground surface to an RC pile cap. The bridges surveyed closely resembled designs found in the FHWA Standard Plans. Schematics of the typical timber pile bent and superstructure are shown in Fig. 1.

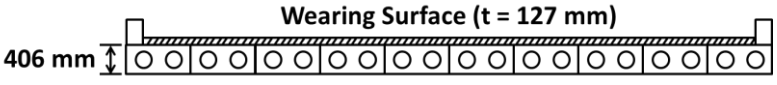

a)

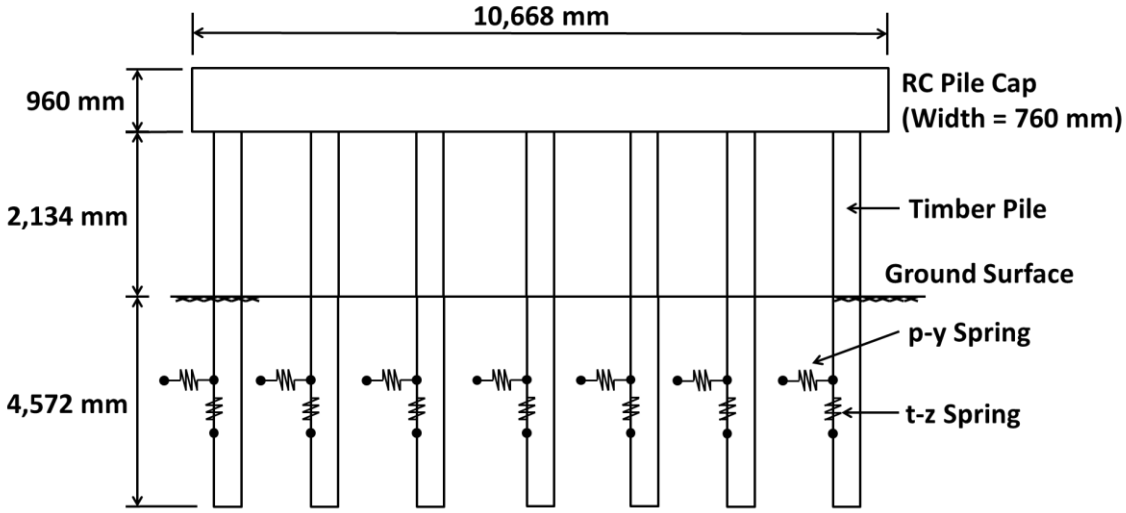

b)

Fig. 1 – a) Typical precast concrete slab-beam superstructure b) Typical timber pile bridge bent

The timber piles in the analysis were assumed to be round red oak piles 305 mm in diameter. Red oak is a common species used for heavy timber applications such as piles and railroad crossties. The stress-strain behavior of timber is similar to that of concrete. The compression behavior of timber in the direction parallel to the grain is very ductile with a linear relationship up to approximately two-thirds of the peak stress. In tension, timber behaves linearly up to brittle fracture [9]. In OpenSees, the Popovics concrete material (Concrete04) was used to describe the stress-strain behavior of the timber piles. The compressive stress-strain relationship is compared to experimental test results of red oak timber pile specimens in Fig. 2.

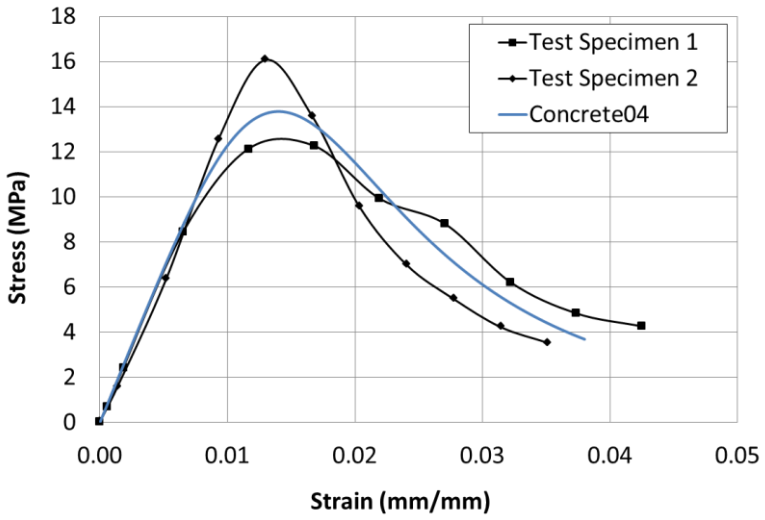

Fig. 2 – Red oak timber pile compressive behavior

The Concrete04 model accurately captures the nonlinear compressive stress-strain relationship observed in the experimental test results. A similar modeling approach was adopted in [10]. The peak stress in tension was assumed to be 10.34 MPa which corresponds to approximately 75% of the peak compressive stress. Due to the presence of defects, timber is generally weaker in tension than in compression. The performance of timber piles is

significantly affected by the ratio of tension to compression strength. The timber piles were discretized into 152 mm nonlinear beam-column finite elements with fiber sections.

As shown in Fig. 1 the soil-pile interaction was modeled using discrete soil springs. The springs were modeled using zero-length elements in OpenSees and applied along the embedded length of the timber piles at each node. The stiffness characteristics of the soil springs were adopted from [11]. A trilinear force-deflection relationship was adopted for the p-y springs. The t-z springs were assumed to behave an elastic-perfectly plastic manner with the yield force varying with depth.

The bridge deck and pile cap were modeled as rigid elements in OpenSees. The deck was assumed to be the same width as the pile cap width with an out-of-plane span length of 9.357 m. The gravity loads from self-weight and live loads were applied as distributed loads along the width of the deck. The mass of each structural component in the model was distributed at each node in the finite element mesh. The out-of-plane depth of the pile cap and the deck are represented in the respective nodal masses. The span length and mass are critical components of the PFEM tsunami analysis.

Although this paper specifically focuses on the response of timber pile bridges, heavy timber piles are also commonly used to support elevated low-rise coastal buildings (e.g. beach houses), and marine and port structures that may be at greater risk from earthquake-tsunami events. It is important to note that the analysis approach discussed in this paper is in no means limited to timber structures and can be applied to a wide range of materials and structures.

3. FRP Retrofitting of Bridge Timber Piles

Currently there is no design guideline available for the design of FRP retrofits for timber structures. A simplified elastic design method for designing full FRP wraps for round timber piles was developed by Caiza et al. (2012) [4]. The method is based on providing adequate FRP reinforcement to restore the flexural stiffness of a degraded timber pile to that of sound timber. The tensile strength of timber is neglected. The number of FRP layers required, n, is calculated as

$$n = \frac{D}{2t}\left(\left(1 + \left(1 - \frac{I_{comp}}{I}\right)\frac{E_{timber}}{E_{FRP}}\right)^{\frac{1}{4}} - 1\right) \quad (1)$$

where, D is the timber pile diameter, t is the thickness of a single layer of FRP composite, I is the moment of inertia of the complete timber pile section, I_{comp} is the effective moment of inertia of the timber pile section neglecting timber tensile strength, and E_{Timber} and E_{FRP} are the Young's moduli for the timber pile and FRP composite, respectively. Several unretrofitted red oak timber pile specimens were tested in flexure-compression by Caiza et al. (2012) to determine their elastic moduli then Eq. (1) was used to compute the FRP thickness necessary to retrofit them. Using a 0.6 mm thick glass-FRP (GFRP) composite with a Young's modulus of 12,400 MPa, it was determined that most of the piles required 8 or 9 layers of GFRP composite to restore their flexural stiffness.

To model an FRP retrofitted timber pile in this study, two 280 mm diameter red oak timber pile specimens were wrapped with 10 layers of GFRP composite and tested in uniaxial compression. The specimens were 610 mm in length. The same GFRP composite as in [8] was used. Similar to the unretrofitted specimens, the FRP wrapped timber pile behavior was also modeled in OpenSees using the Concrete04 material model. The Concrete04 FRP retrofitted timber pile material model is compared to the test results in Fig. 3.

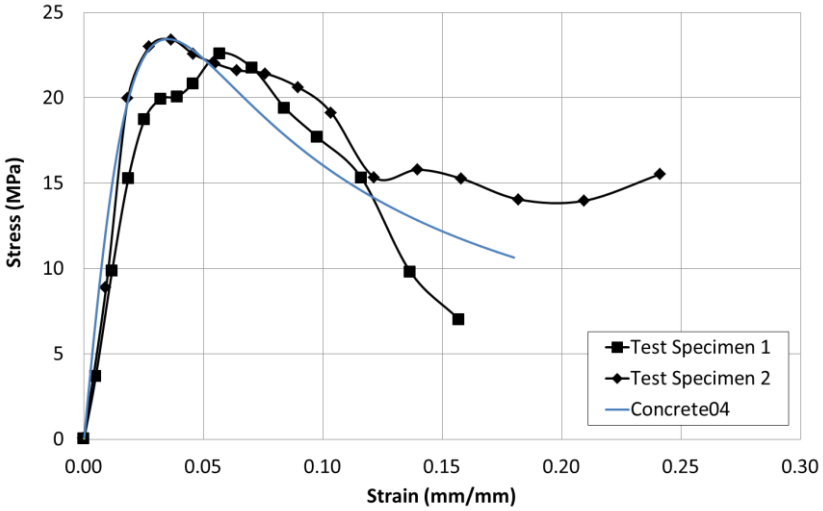

Fig. 3 – Compression behavior of red oak timber pile retrofitted with 10 layers of GFRP composite

As can be seen, FRP retrofitting greatly improves the strength and ductility of timber piles. In this study, it was assumed that all seven timber piles in the bent model are retrofitted with 10 layers of GFRP composite from the ground surface to the pile cap. Unlike concrete members whose behavior can be determined at a smaller scale using cylinder specimens it is not possible to test heavy timber specimens at such levels. Although the behavior shown in Fig. 3 is representative of a full timber pile specimen, the stress-strain behavior was assigned at the fiber level in the finite element model. Therefore, the overall timber pile model will exhibit a smoothed material behavior. FRP confinement does not directly affect the tensile behavior of the timber piles. In both the unretrofitted and retrofitted cases, the material behavior is not dependent on the loading. Variations in the loading will be reflected in the distribution of the stress in the fibers (e.g. uniaxial compression versus combined axial-flexure).

The pile section below the ground surface was assumed to be unretrofitted. A timber pile bent model with unretrofitted timber piles and one with retrofitted timber piles were subjected to the same earthquake-tsunami loading scenario and the results were compared.

4. Earthquake Ground Motion and Tsunami

The earthquake-tsunami loading scenario adopted in this study is from the 2011 Tohoku Earthquake. In many cases, it is difficult to accurately estimate tsunami inundation depth and flow velocity due to logistical and geographical complexities. The investigation by Fritz et al. (2012) used light detection and ranging (LiDAR) to determine the tsunami height and velocity directly from video footage taken by survivors at Kesennuma Bay [12]. Since this information is available, the earthquake ground motion from a seismometer located in Kesennuma was adopted. The acceleration-time history for the March 11th, 2011 earthquake recorded at Kesennuma Station (MYG001) is shown in Fig. 4.

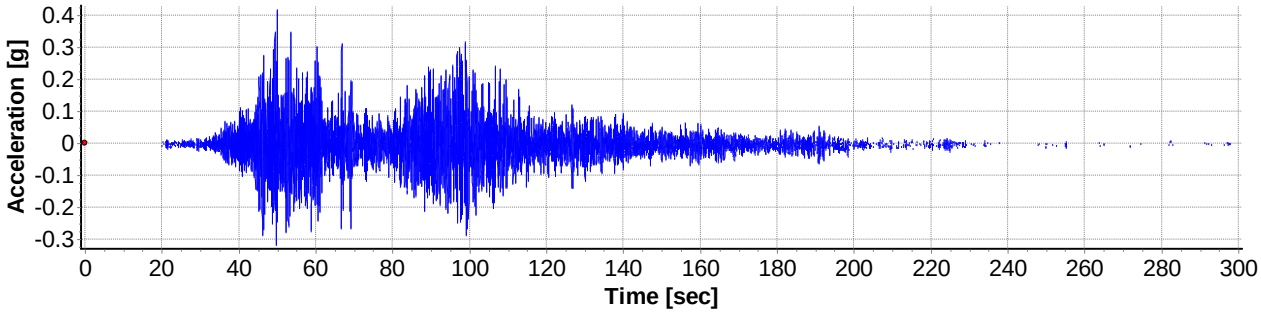

Fig. 4 – Acceleration-time history of the 2011 Tohoku Earthquake recorded at Kesnnuma Station

The ground motion record shown in Fig. 4 has a peak ground acceleration (PGA) of 0.42 g and an Arias Intensity of 9.86 m/sec. The acceleration-time series was truncated down to the significant duration ($D_{5\text{-}95}$) (approximately 90 seconds). Given the extremely high intensity of the ground motion, the acceleration record was scaled down by a factor of 0.25 in OpenSees.

An idealized bore is a simple but effective way to model a tsunami flow. Paczkowski (2011) suggests the relationship between the tsunami bore height and velocity can be described well by Froude scaling [13]. The tsunami bore in this study was defined in a manner similar to the study by Carey et al. (2014) [7]. The tsunami loading analysis set up defined in OpenSees is illustrated in Fig. 5.

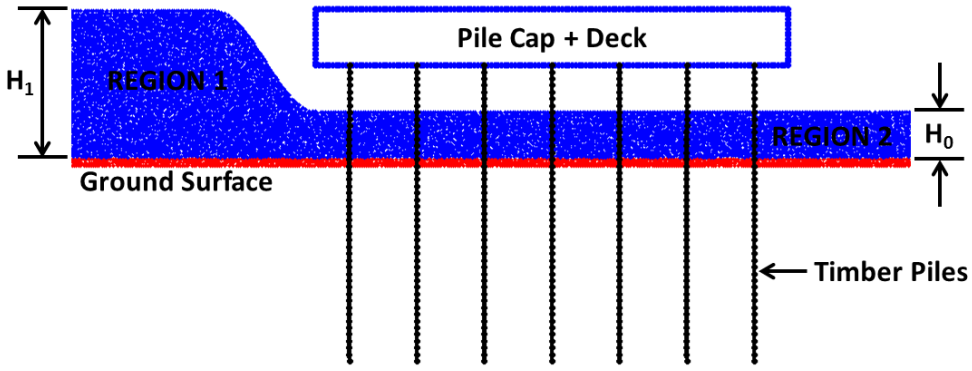

Fig. 5 – Tsunami simulation setup

The tsunami bore is defined by two regions. Region 1 is the bore with height H_1 and a prescribed initial velocity. Region 2 corresponds to the downstream standing water with height H_0 where the initial velocity is zero. The depth of Region 2 was taken to be 1.067 m which corresponds to half of the timber pile height above the ground surface. The tsunami bore velocity (U) is related to H_0 by the Froude number (F_r) as

$$F_r = \frac{U}{\sqrt{gH_0}} \tag{2}$$

where g is the gravitational acceleration. As noted in Carey et al. (2014) the ratio of H_1 to H_0 must be between 2.0 and 2.6 to ensure a fully developed bore. In this study, an H_1/H_0 ratio of 2.6 was adopted which yields a bore height H_1 of 2.77 m. To maintain a consistent bore strength with varying velocities and bore height, a constant Froude number of 1.43 was used. Given these parameters, the initial tsunami bore velocity was computed to be 4.6 m/sec.

5. PFEM Analysis

Since first being developed, the Particle Finite Element Method (PFEM) has been shown to be an accurate and versatile numerical method especially useful for solving fluid-structure interaction (FSI) problems. PFEM uses the Lagrangian formulation for both the fluid and structure. The key feature of the PFEM is to assign all physical and mathematical properties to the mesh nodes which are treated as lumped material particles. Each analysis time step begins by generating a finite element mesh to connect the particles using Delaunay tessellation. The boundaries of the analysis domains are then identified using the Alpha Shape Method [14]. This monolithic treatment of fluid and solid particles allows for a very intuitive and natural coupling of the two materials. Standard FEM solution methods are used to solve the discretized governing equations. Recently, the OpenSees framework was extended to include PFEM analysis capabilities by Zhu and Scott (2014) [6].

Prior to the tsunami simulation, impermeable flow boundaries are defined at the ground surface and behind the tsunami bore in order to direct the flow toward the timber pile bridge. The flow boundaries are outlined in red in Fig. 5. The boundary prevents the tsunami flow from directly interacting with the embedded portions of the timber piles and soil springs. The tsunami bore is discretized into a mesh with 75 mm × 75 mm elements. As discussed above, the out-of-plane span length is 9.357 m. This is the contact width over which the tsunami flow interacts with the timber pile bent. Since the timber piles are relatively narrow compared to the out-of-plane thickness of the pile cap and deck, the interaction of the tsunami with the timber piles is neglected. The response of the timber pile bent will be dominated by the impact of the tsunami bore with the pile cap-deck assembly. To facilitate accurate coupling between the fluid and the pile cap/deck nodes, the pile cap and deck were meshed with elements identical in size to the fluid elements.

6. Multi-Hazard Simulation

The analysis of the timber pile bridge bent under earthquake-tsunami loading consists of several different model definition and analysis steps. An approach similar to the analysis framework developed by Carey et al (2014) was adopted [7]. The analysis proceeds as follows:

- Step 1: Generate timber pile, pile cap, and deck elements.
  Define and assign material properties, sections, and nodal masses.
- Step 2: Apply dead loads.
- Step 3: Create soil springs using zero-length elements and connect to the timber pile nodes below the ground surface.
- Step 4: Apply live loads.
- Step 5: Earthquake simulation.
- Step 6: Perform critically damped free analysis to remove free vibrations prior to the tsunami simulation. This is done by changing the Newmark time integration parameters β, and γ to 1.5 and 1.0 respectively which introduces numerical damping [4].
- Step 7: Define the fluid boundary using 2D PFEM elements.
  Fix all boundary nodes against translation.
- Step 8: Define the tsunami bore and discretize into PFEM elements.
- Step 9: Prescribe initial tsunami bore velocity.
- Step 10: Tsunami simulation.

The pile head lateral deformation response for the timber pile at the left end of the pile cap (tsunami side of the bridge) to the seismic excitation is plotted in Fig. 6. The unretrofitted and retrofitted timber pile cases are compared.

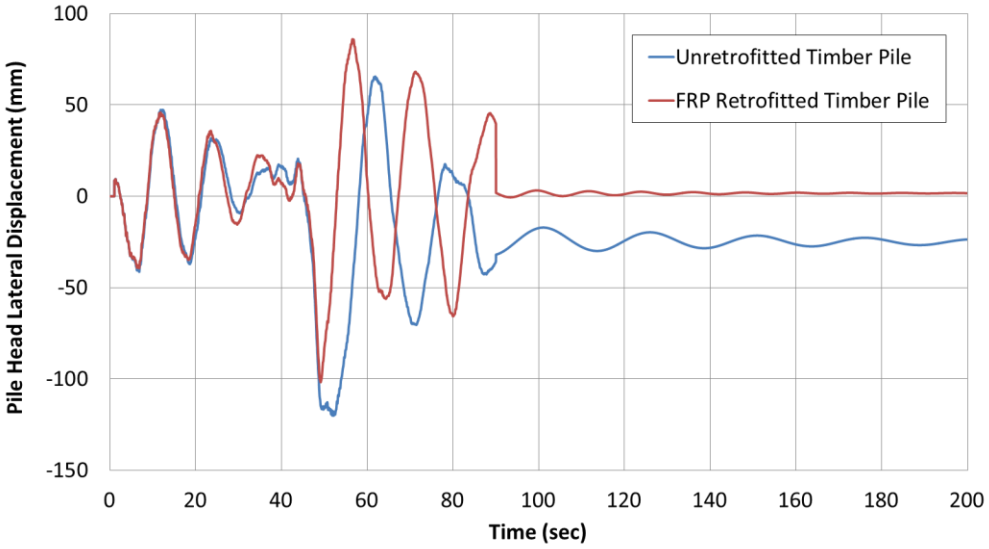

Fig. 6 – Pile head lateral displacement-time history for the timber pile at the left end

The difference between the performance of the unretrofitted and FRP retrofitted timber piles is clear in the residual deformation. In the unretrofitted case, the earthquake loading leads to a residual lateral deformation of approximately 26 mm. In comparison, the residual deformation in the FRP retrofitted timber piles is less than 2 mm. This is indicative of the improvement in stiffness and strength provided by the FRP.

Once the earthquake and free vibration analyses are complete, the tsunami analysis is carried out with the timber pile bent in its plastically deformed shape. To maximize the damage to the timber piles, the tsunami bore was set up such that the flow would deform the structure further in the direction of the residual displacement. The sole purpose of this was to simply maximize the damage in the timber piles. In this study, the tsunami analysis was only carried out for 2 seconds. This is adequate simulation time to observe the effects of the tsunami impact. The tsunami simulation with unretrofitted timber piles at time 0 and at 1 second are shown in Fig. 7.

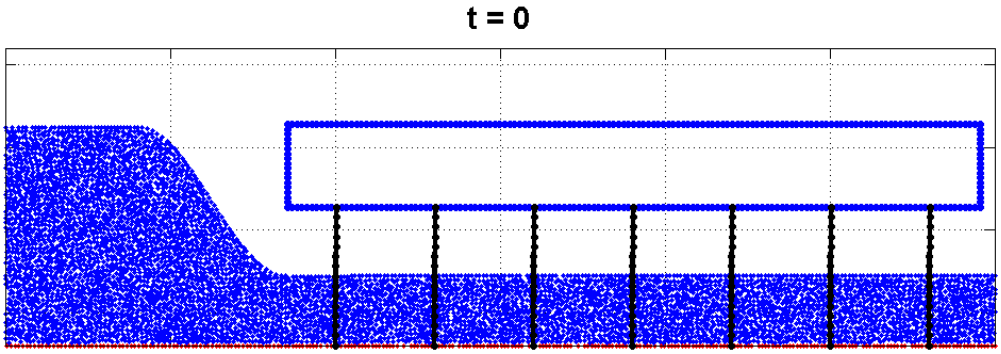

a)

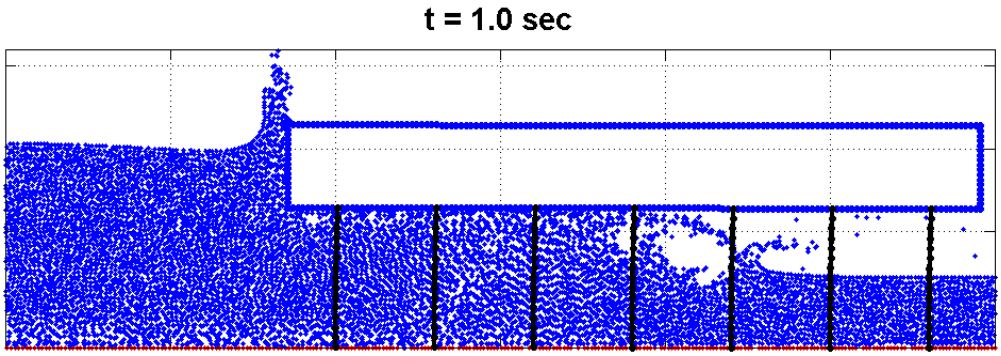

b)

Fig. 7 – a) Tsunami simulation at t = 0 b) Tsunami simulation at t = 1.0 sec

Although not clearly visible in Fig. 7, the tsunami simulation begins with the residual deformation from the earthquake analysis. The residual deformation in the unretrofitted timber piles was such that the bent is leaning away from the tsunami. In Fig. 7 b) the tsunami impact can be seen further amplifying the lateral displacement. The lateral pile head deformation of the timber pile at the left end due to the tsunami loading is plotted in Fig. 8.

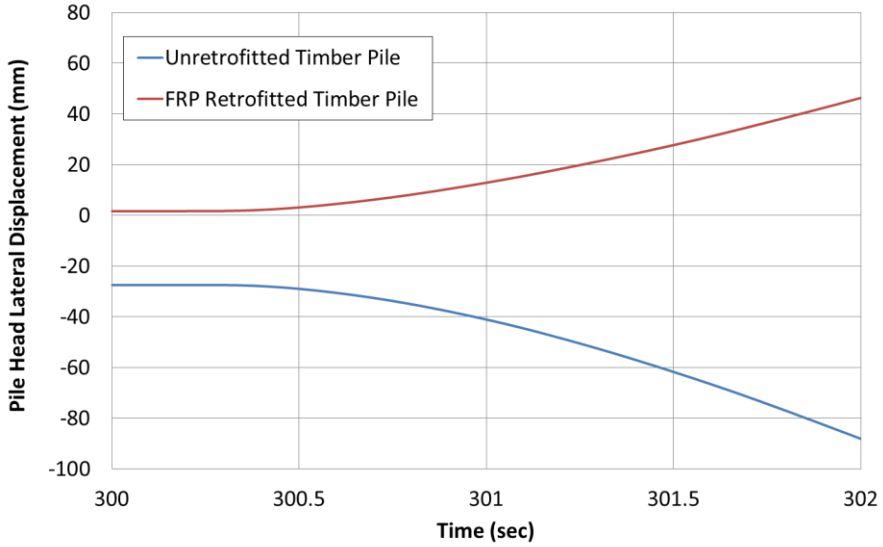

Fig. 8 – Pile head lateral displacement-time history for the timber pile at the left end

As shown in Fig. 8 the lateral displacement response to the tsunami loading is relatively smooth. The tsunami pushes the timber piles in the direction of the flow. As was the case in the earthquake simulation, the FRP retrofitted piles are stiffer. At the end of the tsunami simulation, the total lateral pile head displacement relative to the residual deformation at the end of the earthquake simulation is 61 mm in the unretrofitted timber pile and 45 mm in the FRP retrofitted timber pile. At these drift levels it is expected that the extreme tensile fibers in the timber piles will approach the modulus of rupture. Most of the damage will be concentrated near pile-pile cap joint. In order to determine the residual deformation in the timber piles at the end of the tsunami simulation a significantly longer simulation time is needed to allow the fluid to settle to a steady state. It is important to note that in addition to lateral deformation, significant uplift forces are generated by the tsunami flow.

7. Conclusions

Timber pile bridges are vulnerable to damage from extreme loading scenarios due to poor design and problems posed by deterioration. Retrofitting timber piles with FRP composites has been shown to be effective at improving the stiffness and strength. This study compared the response of unretrofitted and FRP retrofitted bridge timber piles subjected to an earthquake-tsunami multi-hazard event. The OpenSees analysis framework was used to perform the analyses in sequential fashion. Earthquake ground motion and tsunami data from the 2011 Tohoku Earthquake event recorded at Kesennuma Bay were used. The damage caused by the loads imposed by each hazard was quantified by the resulting level of inelastic deformation.

Overall, the behavior of the retrofitted timber piles was much stiffer than that of the unretrofitted timber piles. The residual lateral deformation in the unretrofitted timber pile caused by the earthquake ground motion was more than 13 times higher than the FRP retrofitted timber pile. At the end of a 2 second tsunami simulation the total lateral displacement in the unretrofitted timber pile approximately 36% higher than the FRP retrofitted timber pile. These results provide a glimpse of the lack of robustness in typical timber pile bridges and show how effective FRP retrofits can be.

The analysis approach adopted in this study will be used to analyze timber pile bridges under a suite of multi-hazard scenarios. The bridge geometric parameters will be varied as well as incorporating timber pile deterioration in future analyses to develop multi-hazard interaction diagrams. The ultimate goal is that these diagrams can provide a tool that a governing agency can use to obtain performance estimates or make repair or retrofitting decisions for a given bridge layout and the level of deterioration.

8. Acknowledgements

This work was supported by the Illinois Center for Transportation and the Illinois Department of Transportation (ICT/IDOT) under project No. R27-134 and by the UIUC CEE Innovation Grant. The authors would also like to Thank Dr. Armando C. Duarte at the University of Illinois at Urbana-Champaign for his input and Dr. Minjie Zhu and Dr. Michael Scott at Oregon State University for their assistance with PFEM in OpenSees.

9. References

[1] Hagos, M. W. (2001). Repair of heavily decayed timber piles using glass fiber-reinforced polymers (GFRP) and cementitious grout. *M.S. Thesis*, University of Manitoba, Winnipeg, Manitoba, Canada.

[2] Andrawes, B., & Caiza, P. (2011). Bridge Timber Piles Load Rating under Eccentric Loading Conditions. *Journal of Bridge Engineering*, *17*(4), 700-710.

[3] Plevris, N., & Triantafillou, T. C. (1992). FRP-reinforced wood as structural material. *Journal of materials in Civil Engineering*, 4(3), 300-317.

[4] Caiza, P., Shin, M., & Andrawes, B. (2012). Flexure-Compression Testing of Bridge Timber Piles Retrofitted with Fiber Reinforced Polymers. *Open Journal of Civil Engineering*, *2*(03), 115.

[5] McKenna F, Fenves GL, Scott MH. Open system for earthquake engineering simulation. Berkeley, CA: University of California; 2000. Available from: http://opensees.berkeley.edu.

[6] Zhu, M., & Scott, M. H. (2014). Modeling fluid–structure interaction by the particle finite element method in OpenSees. Computers & Structures, 132, 12-21.

[7] Carey, T., Mason, H. B., Barbosa, A. R., & Scott, M. H. (2014). Modeling framework for soil-bridge system response during sequential earthquake and tsunami loading. *Tenth US National Conference on Earthquake Engineering, Anchorage, AK*

[8] Shama, A. A., & Mander, J. B. (2003). The seismic performance of braced timber pile bents. *Earthquake engineering & structural dynamics*, *32*(3), 463-482.

[9] Buchanan, A. H. (1990). Bending strength of lumber. *Journal of structural Engineering*, *116*(5), 1213-1229.

[10] Shama, A. A., Mander, J. B., Friedland, I. M., & Allicock, D. R. (2007). Seismic vulnerability of timber bridges and timber substructures. (No. MCEER-07-0008).

[11] Borello, D. J., Andrawes, B., Hajjar, J. F., Olson, S. M., & Hansen, J. (2010). Experimental and analytical investigation of bridge timber piles under eccentric loads. *Engineering Structures*, *32*(8), 2237-2246.

[12] Fritz, H. M., Phillips, D. A., Okayasu, A., Shimozono, T., Liu, H., Mohammed, F., ... & Takahashi, T. (2012). The 2011 Japan tsunami current velocity measurements from survivor videos at Kesennuma Bay using LiDAR. *Geophysical Research Letters*, *39*(7).

[13] Paczkowski, K. (2011). Bore impact upon vertical wall and water-driven, high-mass, low-velocity debris impact. *Dissertation Abstracts International*, *73*(182), 2011.

[14] Oñate, E., Idelsohn, S. R., Del Pin, F., & Aubry, R. (2004). The particle finite element method—an overview. International Journal of Computational Methods, 1(02), 267-307.